Effects of nonuniform reflective boundaries and line competition on radiation trapping

T. M. Colbert* and B. L. Wexler
Naval Research Laboratory, Washington, D.C. 20375
(Received 9 April 1992)

We develop a radiation diffusion equation for an infinite slab geometry where the slab may have different reflectivities on either surface, and for conditions where complete frequency redistribution is valid. Additionally we consider the effect of two competing trapped transitions. Specifically we consider the emission from the thallium $7\,^2S_{1/2}$ state to either the $6\,^2P_{3/2}$ (metastable state) at 535 nm or $6\,^2P_{1/2}$ (ground state) at 378 nm. High densities of the long-lived metastable level can be produced in a number of ways. The escape factors (which are simply related to the decay rates) and excited-atom spatial profiles are calculated for a variety of conditions for the first several natural modes of the system. The spatial modes for this system are asymmetric. The asymmetry can vary dramatically with only small changes in either of the two lower-state densities. The correct description of the spatial modes is critical in order to determine the overall excited-atom profile accurately. For the simpler systems (i.e., a single transition and nonreflective boundaries) usually considered the mode profiles do not change appreciably as the optical depth is changed (given conditions of high optical depth and a single-line broadening mechanism). The fundamental mode decay rate is shown for a fixed metastable-state density as a function of the ground-state density. The dependence of the fundamental mode escape factor for the first resonance transition on the optical depth (or ground-state density) is in general more complicated than for the case of a single trapped transition. For conditions considered here a simple power rule cannot be used to scale the decay rates as a function of line-center optical depth. Also shown is the fundamental mode escape factor as a function of buffer gas pressure for fixed ground- and metastable-state densities. The calculations presented here allow us to model the narrow-bandwidth thallium fluorescence filter. This filter will be discussed in more detail in a separate paper. A thorough review of atomic resonance filters was done by Gelbwachs [IEEE J. Quantum Electron. **24**, 1266 (1988)]. We have considered a much broader range of ground- and metastable-state densities than would be practical for efficient filter operation. This is done to illustrate several aspects of the radiation trapping processes.

PACS number(s): 32.50.+d, 32.90.+a

I. INTRODUCTION

The transport of resonance radiation has been studied in a number of experimental and theoretical papers [1–23]. A variety of techniques may be used to describe the diffusion of resonance radiation in systems of increasing complexity. The earlier treatments of Milne [1] used an average absorption and emission coefficient for the gas. This type of solution has been shown to be valid for only a limited set of conditions at low optical depth [21]. Later developments by Holstein [2,3] showed that a more complete description was given by his radiation diffusion equations for conditions where complete frequency redistribution for the reemitted photon is a valid assumption. More recently, several papers have been written that derive Holstein-like radiation diffusion equations that include the effects of incomplete frequency redistribution [10,11,14–16].

The various radiation diffusion treatments discussed above allow solutions to be obtained for a wide variety of conditions. Holstein derived solutions for conditions of high optical depth, ideal geometry, complete frequency redistribution, and a single line-broadening mechanism [2,3]. Holstein's simple analytic solutions [2,3] are particularly easy to use, and have been shown to predict decay rates that are in good agreement with experimentally measured decay rates for the appropriate set of conditions. Several more complicated numerical calculations have been performed in order to examine conditions of incomplete frequency redistribution and low to moderate optical depths [10,11,14,15,20]. Additionally, more complicated cell boundary conditions have been considered. Solutions for conditions where the cell boundaries are uniformly partially reflective have been examined numerically [5,7,8].

We derive a Holstein-like equation for conditions where the reflectivity on the cell boundary (we consider only the infinite slab geometry here) is nonuniform both spatially and in frequency (wavelength). We also discuss numerical solutions to a specific case for this geometry which includes the effects of two trapped transitions. The specific case we consider is for an infinite slab geometry with a different reflectivity on each of the two walls. The problem can then be reduced to a one-dimensional problem spatially. The techniques may be extended to more complicated geometries. However, this may lead to intractable numerical problems. Additionally, we consider radiation trapping under conditions of line competition (i.e., more than one trapped transition depletes the excited state via radiation). Complete frequency redistribution is assumed to be valid. In principle, partial frequency redistribution can be accounted for

as described in Refs. [10,11,14–16], but the solutions to the resulting radiation diffusion equation are expected to be extremely complicated when coupled with the nonuniform reflectivities and multiple trapped transitions. We note that typically the cells are considered to have 0% reflectivity at the boundaries. Even a uniform reflectivity applied to all surfaces of a cell with ideal geometry makes the radiation diffusion problem quite complicated [5,7,8]. The infinite slab geometry considered here has only the two surfaces; the other surfaces which must exist in real cells can be made 100% reflecting so that the laboratory cell approximates an infinite slab cell.

II. THEORY

A. General development

The present derivation follows much of the treatment of the radiation diffusion problem developed by Weinstein [5]. Weinstein derived a "generalized-Holstein" equation to describe radiation diffusion under conditions of uniformly reflective boundaries. Weinstein considered spherical, cylindrical, and infinite slab geometries. We consider the infinite slab geometry only. The present discussion will extend Weinstein's work by deriving a radiation diffusion equation for a cell with two different reflectivities on either side of an infinite slab geometry (see Fig. 1). In principle, the reflectivity can vary in a more complicated manner, but the problem may then be intractable for all practical purposes. Complete frequency redistribution is also assumed in this derivation. That is, the emission profile is assumed to be the same as the absorption line profile. The additional complication of line competition between two or more trapped transitions depleting the same excited state will be discussed later in this section. Note that the problem must consider $2n$ different reflectivities when n trapped transitions are considered. For the case to be discussed later in this paper, we consider only two such transitions; thus, Fig. 1 shows four different reflectivities (the reflectivity is considered constant over the narrow frequency range about each line where emission occurs).

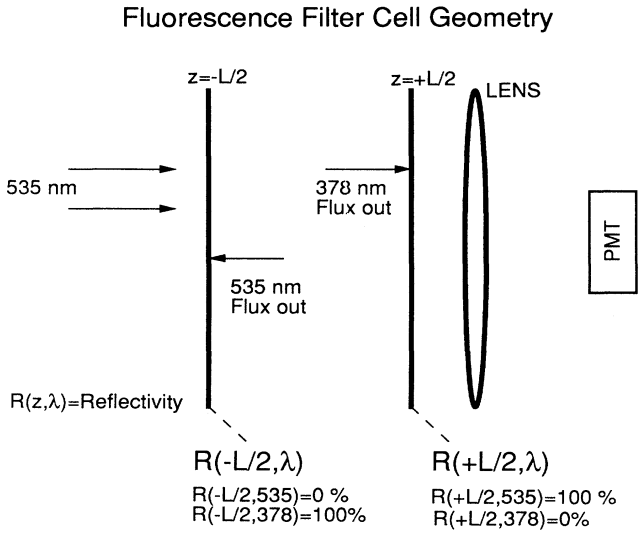

FIG. 1. The cell shown here applies the thallium fluorescence filter which emits light at both 535 and 378 nm. Four reflectivities are required to describe the cell for a general set of reflectivities. The results shown here are for the special case where at $-L/2$ we have $R(-L/2,535\ \text{nm})=0$ and $R(-L/2,378\ \text{nm})=100\%$, and on the $+L/2$ wall we have converse conditions with $R(+L/2,378\ \text{nm})=0$ and $R(+L/2,535\ \text{nm})=100\%$. For the single-line case, simply omit either transition, and the cell is described by only two reflectivities. Likewise, for n trapped transitions the cell is described by $2n$ reflectivities. The lens and photomultiplier tube (PMT) represent a simplified detection system.

We derive the kernel $[G(\mathbf{r},\mathbf{r}')]$ for a Holstein-like radiation diffusion equation in the following form:

$$\frac{\partial n(\mathbf{r},t)}{\partial t}=-A_\lambda n(\mathbf{r},t)+A_\lambda\int G(\mathbf{r},\mathbf{r}')n(\mathbf{r},t)d^3\mathbf{r}'+\left[\frac{dn(\mathbf{r},t)}{dt}\right]_i . \quad (1)$$

Here,

$$G(\mathbf{r},\mathbf{r}')=G_0(\mathbf{r},\mathbf{r}')+G_R(\mathbf{r},\mathbf{r}') ,$$

$G_0(\mathbf{r},\mathbf{r}')$ is the standard Holstein kernel to be given below [2,3], and $G_R(\mathbf{r},\mathbf{r}')$ is the contribution due to the reflective boundaries to be derived here. Since the standard Holstein kernel is discussed in many references [2,3,5] we focus on the $G_R(\mathbf{r},\mathbf{r}')$ term. $G(\mathbf{r},\mathbf{r}')d^3\mathbf{r}'$ is the probability that a photon emitted in the volume element about $\mathbf{r}'$ is absorbed at $\mathbf{r}$. A_λ represents the spontaneous emission rate for the transition being considered, $n(\mathbf{r},t)$ is the excited-atom density, and $[dn(\mathbf{r},t)/dt]_i$ is a source term. The source term refers to the creation of "the excited state" by any process (for the case we consider this is the $7S$ state in thallium). We consider cases where the source term is constant in time. Equation (1) is given for a single trapped transition, and the extension to several trapped transitions will be made later in this paper. Since we consider the effects of several trapped transitions, we note that the only state to be considered "the excited state" is that described by $n(\mathbf{r},t)$. Since emission may be to any number of lower states, all but one of which (the ground state) are in fact also excited states, we will try to maintain a clear distinction. The notation used by Weinstein is followed here as much as possible. We note that transit-time effects are negligible here due to the small size of the vapor cells considered. The actual results to be presented here are for a slab geometry explicitly. For this problem, Eq. (1) can be expressed in terms of one spatial variable, usually z, rather than $\mathbf{r}$. That is, for the slab geometry with the boundary conditions to be used here, Eq. (1) can be integrated over both x' and y'. However, we present the theory in terms of $G(\mathbf{r},\mathbf{r}')$ for completeness. When written in terms of z only, $G(\mathbf{r},\mathbf{r}')$ is usually replaced by $K(z,z')$. $K(z,z')$ simply incorporates the integrals over the x' and y' coordinates in Eq. (1).

For conditions of complete frequency redistribution, the following Boltzmann photon equation can be derived [5,9,16]:

$$\omega\cdot\mathrm{grad}_{\mathbf{r}}[f(\mathbf{r},\omega,\nu)]+k(\nu)f(\mathbf{r},\omega,\nu)=\frac{k(\nu)n(\mathbf{r},t)}{4\pi\kappa c A_\lambda} , \tag{2}$$

where $f(\mathbf{r},\omega,\nu)d^3\mathbf{r}\,d^2\omega\,d\nu$ is the number of resonance photons in the volume element about $\mathbf{r}$ in the frequency interval about ν traveling in the direction ω. We note that the time dependence of $f(\mathbf{r},\omega,\nu)$ simply follows the exited-form distribution $n(\mathbf{r},t)$ and will not be explicitly written throughout this paper. The absorption coefficient at frequency ν is $k(\nu)$, and κ is the line normalization [that is, $\int k(\nu)d\nu=\kappa$].

Weinstein wrote out the following equation of continuity which is valid for the conditions discussed in this paper:

$$\frac{\partial n(\mathbf{r},t)}{\partial t}=-A_\lambda n(\mathbf{r},t)+A_\lambda\int ck(\nu)f(\mathbf{r},\omega,\nu)d\nu\,d^2\omega + \left[\frac{dn(\mathbf{r},t)}{dt}\right]_i . \tag{3}$$

We refer the reader to Weinstein's Eqs. (1)–(6) for a discussion of Eqs. (2) and (3) shown above. The solution we week is the function $n(\mathbf{r},t)$. In order to solve Eqs. (2) and (3), we must find a relation between the function $f(\mathbf{r},\omega,\nu)$ (which is related to the intensity [16]) and the excited-atom profile. The absorption profile, A_λ coefficients, and geometry are assumed to be known.

Weinstein wrote out the following boundary conditions for an enclosure as viewed from the inside with a diffuse reflectivity $R(\mathbf{r}_b)$. The enclosure must be nonreentrant. The diffuse reflectivity assumption simplifies the boundary conditions significantly and is also a good approximation to specular reflectivity for conditions of high or low optical depths. For conditions of high optical depth, the photon is scattered again after reflection very near the surface; thus the wall appears as a diffuse reflector to most of the cell. For conditions of low optical depth, the angular distribution of reflected light is nearly uniform since the probability of absorption is low regardless of direction. The difference in the results for these two types of boundary conditions in the moderate optical depth regime is expected to be small since the transition from high to low optical depth regions occurs over a narrow range of optical depth [21].

The reflection is assumed to take place without redistribution of the frequency. Then if $\mathbf{n}_b$ is an outward normal unit vector at a boundary point $\mathbf{r}_b$, the photon flux $cF(\mathbf{r}_b,\nu)$ at the surface is determined by (the flux is the number of photons per unit area with frequency ν, per second, incident upon the surface at the point $\mathbf{r}_b$)

$$F(\mathbf{r}_b,\nu)=\int_{\omega\cdot\mathbf{n}_b>0}\omega\cdot\mathbf{n}_b f(\mathbf{r}_b,\omega,\nu)d^2\omega . \tag{4}$$

For the flux direction into the cell from the surface at $\mathbf{r}_b$ a similar expression can be written, but with $\omega\cdot\mathbf{n}_b<0$. For this integral, the intensity function $f(\mathbf{r},\omega,\nu)$ can be pulled out of the integral, since for a diffuse reflector the reflected intensity is uniform throughout the solid angle. Since the reflectivity, which is known, gives the ratio of reflected to incident flux at the boundary, the intensity function $f(\mathbf{r},\omega,\nu)$ is then given in terms of the flux function $F(\mathbf{r}_b,\nu)$ and the reflectivity by

$$f(\mathbf{r}_b,\omega,\nu)=\frac{R(\mathbf{r}_b)F(\mathbf{r}_b,\nu)}{\pi} , \quad \omega\cdot\mathbf{n}_b<0 . \tag{5}$$

Weinstein then wrote out the intensity function as the solution to the photon Boltzmann equation [Eq. (2)] for the boundary conditions of [Eq. (5)]:

$$f(\mathbf{r},\omega,\nu)=\frac{R(\mathbf{r}'_b)F(\mathbf{r}'_b,\nu)}{\pi}\exp[-k(\nu)|\mathbf{r}-\mathbf{r}'_b|] + \frac{A_\lambda}{4\pi\kappa c}\int_0^{|\mathbf{r}-\mathbf{r}'_b|} n(\mathbf{r}-\omega\rho,t) \times\exp[-k(\nu)\rho]d\rho , \tag{6}$$

where $\mathbf{r}'_b$ is the boundary point in the direction ω from the point $\mathbf{r}$ such that

$$\omega=\frac{(\mathbf{r}-\mathbf{r}'_b)}{|\mathbf{r}-\mathbf{r}'_b|} . \tag{7}$$

This solution shown in Eq. (6) contains two terms: The first accounts for the wall reflectivities and the second is the standard Holstein term accounting for the diffusion throughout the volume of vapor. Note that the nature of $R(\mathbf{r}_b)$ is still completely general. [The wavelength dependence has been left out of $R(\mathbf{r}_b)$ at this point since we only need to consider a single transition for this part of the derivation. The reflectivity is assumed to be constant over the narrow frequency range of a single transition. The generalization to several trapped transitions will be discussed later. For that case we consider a different reflectivity for each transition $R(\mathbf{r}_b,\lambda)$.] Equation (6) describes the photon distribution (for a given frequency photon traveling in a given direction) at a point $\mathbf{r}$ in terms of the flux incident on the boundary at the related boundary point (the boundary point at which a reflected photon originated) and the excited-atom distribution along the line from the boundary point $\mathbf{r}'_b$ to $\mathbf{r}$. The intensity function $f(\mathbf{r},\omega,\nu)$ depends on two unknown functions $F(\mathbf{r}_b,\nu)$ and $n(\mathbf{r},t)$. In order to solve the problem using a Holstein-like equation, the flux incident on the boundary must be written in terms of the excited-atom distribution $n(\mathbf{r},t)$. Equation (6) can be transformed so that the left-hand side is written in terms of the flux as follows. Following Weinstein's approach [5], we set $\mathbf{r}=\mathbf{r}_b$ in Eqs. (6) and (7), then multiply by $\omega\cdot\mathbf{n}_b$, and integrate over all solid angles with $\omega\cdot\mathbf{n}_b>0$. The solid angle can be represented as an element of surface area at the boundary:

$$d^2\omega=\frac{|\omega\cdot\mathbf{n}'_b|}{|\mathbf{r}_b-\mathbf{r}'_b|^2}dS'_b . \tag{8}$$

$\mathbf{n}'_b$ is outward normal at the boundary point $\mathbf{r}'_b$. The resulting integral equation for $F(\mathbf{r}_b,\nu)$ is then

$$F(\mathbf{r}_b,\nu)=F_0(\mathbf{r}_b,\nu)+\int I(\mathbf{r}_b,\mathbf{r}'_b)R(\mathbf{r}'_b)F(\mathbf{r}'_b,\nu)dS'_b . \tag{9}$$

where $I(\mathbf{r}_b,\mathbf{r}'_b)$ and $F_0(\mathbf{r}_b,\nu)$ are defined as follows:

$$I(\mathbf{r}_b,\mathbf{r}'_b)=\frac{|\mathbf{n}_b\cdot(\mathbf{r}_b-\mathbf{r}'_b)||\mathbf{n}'_b\cdot(\mathbf{r}_b-\mathbf{r}'_b)|}{\pi|\mathbf{r}_b-\mathbf{r}'_b|^4}\exp[-k(\nu)|\mathbf{r}_b-\mathbf{r}'_b|]\ , \tag{10}$$

$$F_0(\mathbf{r}_b,\nu)=\frac{A_\lambda k(\nu)}{4\pi\kappa c}\int_{\omega\cdot\mathbf{n}_b>0}\omega\cdot\mathbf{n}_b d^2\omega\int_0^{|\mathbf{r}_b-\mathbf{r}'_b|}n(\mathbf{r}_b-\omega\rho,t)\exp[-k(\nu)\rho]d\rho\ . \tag{11}$$

The surface integral in Eq. (9) is over the entire cell boundary. (Note that in an ideal *infinite slab* geometry the cell has only two surfaces bounding the vapor. The other surfaces which must exist in a real cell do not enter into the radiation diffusion problem. If these surfaces are made 100% reflecting at all relevant wavelengths, then the real cell is a good approximation to an *infinite slab* cell.) Equation (9) represents the flux of photons incident on the boundary at $\mathbf{r}_b$ with frequency ν. The first term in Eq. (9) represents the flux that would be present for that cell with nonreflective boundaries (this represents the flux for the case considered by Holstein). The second term in Eq. (9) accounts for the contribution due to reflections. It is now convenient to transform Eq. (11) into a volume integral with the substitution

$$\mathbf{r}'=\mathbf{r}_b-\omega\rho \tag{12}$$

and writing the volume element as

$$d^3\mathbf{r}'=\rho^2 d\rho\, d^2\omega\ . \tag{13}$$

Then we have

$$F_0(\mathbf{r}_b,\nu)=\frac{A_\lambda\mathbf{k}(\nu)}{\kappa c}\int p(\mathbf{r}_b,\mathbf{r}'_b)n(\mathbf{r}',t)d^3\mathbf{r}'\ , \tag{14}$$

where $p(\mathbf{r}_b,\mathbf{r})$ is given by

$$p(\mathbf{r}_b,\mathbf{r})=\frac{|\mathbf{n}_b\cdot(\mathbf{r}_b-\mathbf{r})|}{4\pi|\mathbf{r}_b-\mathbf{r}|^3}\exp[-k(\nu)|\mathbf{r}_b-\mathbf{r}|]\ . \tag{15}$$

Equation (15) represents the probability per unit boundary area that a photon of frequency ν emitted at $\mathbf{r}$ reaches the boundary point $\mathbf{r}_b$ directly without reflection.

B. Infinite slab geometry with different surface reflectivities

The derivation up to this point is very general. In principle, complicated cell geometries, absorption profiles, or reflectivity can be handled. Now we apply conditions specific to an infinite slab geometry with different reflectivities on either side. On either boundary surface of an infinite slab, the reflectivity is constant (see Fig. 1); R_+ at $+L/2$ and R_- at $-L/2$, where L is the full slab thickness. (The $+$ and $-$ subscripts will refer throughout this paper to the evaluation of functions at $z=\pm L/2$, respectively, or to integrations over the planes located at these positions.) This represents a situation which is still not too complicated. We note that for conditions where there are two or more well-isolated trapped transition frequencies, the reflectivity may vary with frequency as well as position. This effect can be incorporated into the solution to the trapping problem quite easily.

Due to the introduction of nonuniform reflectivity on the boundary of the vapor cell (i.e., there is a different reflectivity on either of the two surfaces), the treatment of the trapping problem no longer parallels that of Weinstein. We also note here that Weinstein made the general assumption that the flux is uniform upon the surface of the enclosure [5]. This is only true if the source term [see Eq. (3)] has the same symmetry as the enclosure. This may not in general be true. Because of this assumption, the validity of Weinstein's solution when applied to systems with uniform reflectivity which involve complicated source term (or pump) geometries needs to be examined. For example, Weinstein's assumption is not valid for fluorescence filters since the source term is clearly not symmetric. Weinstein considered the case where the source term only depends on internal processes, and thus has the symmetry of the cell. Weinstein's treatment is valid (for cells with uniform reflectivity) in the late time following a pulsed excitation regardless of the pump geometry, since in the late time the symmetric fundamental mode describes the spatial profile of excited atoms.

The flux [Eq. (9)] is written with the integration over either boundary surface explicitly separated:

$$F(\mathbf{r}_b,\nu)=F_0(\mathbf{r}_b,\nu)+\int_{+L/2\ \text{surface}}I(\mathbf{r}_b,\mathbf{r}'_{b+})R_+F(r'_{b+},\nu)dS'_b+\int_{-L/2\ \text{surface}}I(\mathbf{r}_b,\mathbf{r}'_b)R_-F(\mathbf{r}'_{b-},\nu)dS'_b\ . \tag{16}$$

The two integrals are over the boundary surfaces at $z=+L/2$ and $-L/2$, respectively (see Fig. 1). Due to the symmetry of the cell, the flux at either surface depends only on the z component of $\mathbf{r}_b$. Thus the flux at either wall is a constant along that surface and can be pulled out of the integral in Eq. (16). We will denote the flux on either surface as $F_\pm$ at $\pm L/2$, respectively (likewise for F_0). The flux on either surface can then be written explicitly as

$$F_\pm=\frac{F_{0\pm}+R_-I_LF_{0\mp}}{1-I_L^2R_\mp R_\pm}\ , \tag{17}$$

where I_L is given by

$$I_L=\int_\pm I(\mathbf{r}_{b\pm},\mathbf{r}'_{b\mp})dS'_b$$
$$=2L^2k(\nu)^2E_3(k(\nu)L)\ , \tag{18}$$

where $E_3(k(\nu)L)$ is the third-order exponential function

given by

$$E_n(x)=\int_x^\infty \frac{\exp(-t)}{t^n}dt \tag{19}$$

for $n=3$.

The F_0 term in Eqs. (16) and (17) represents the flux for the simple Holstein case where the reflectivity is 0% on both sides of the cell. Even in a cell with this symmetry, the flux incident on the two surfaces is not necessarily equal. This depends on both the spatial profile of the source term and overall distribution of excited atoms $n(z,t)$ in Eq. (1).

Since the functions F_{0+} and F_{0-} depend on the unknown excited-atom density function $n(\mathbf{r},t)$, we have accomplished the goal of relating the two unknown functions involved in this problem. That is, the intensity function $f(\mathbf{r},\omega,\nu)$ in Eq. (6) can be written in terms of the unknown excited-atom density.

The flux expressions can be reduced for the case considered here by integrating over the plane parallel to the slab. Designating z as the direction across the slab (see Fig. 1), the x' and y' integrations involved in the flux expressions can be carried out. Due to the symmetry of the problem, the excited-atom profile depends only on the z component (we assume the source term is constant in x' and y'). Performing the integrations in Eq. (14) over x' and y', the flux expressions are given by

$$F_{0\pm}=\frac{k(\nu)^2 A_\lambda}{2c\kappa}\int n(z',t)\sqrt{a'_\pm}\,E_2(k(\nu)\sqrt{a_{\pm'}})dz' , \tag{20}$$

where $a'_\pm$ is given by

$$a'_\pm=(z'\pm L/2)^2 . \tag{21}$$

Using Eqs. (6), (17), and (20), we are able to write the intensity function in terms of the excited-atom profile $n(z,t)$. The result can then be substituted into the continuity equation [Eq. (3)]. Starting with the continuity equation, we substitute Eq. (6) into Eq. (3) and then convert the integral over solid angle to a surface integral:

$$\frac{\partial n(\mathbf{r},t)}{\partial t}=\frac{c}{\pi}\int k(\nu)d\nu\int R(\mathbf{r}'_b)F(\mathbf{r}'_b,\nu)\exp[-k(\nu)|\mathbf{r}-\mathbf{r}'_b|]\frac{|\mathbf{n}'_b\cdot(\mathbf{r}-\mathbf{r}'_b)|}{|\mathbf{r}-\mathbf{r}'_b|^3}dS'_b$$
$$+A_\lambda\int G_0(\mathbf{r},\mathbf{r}')n(\mathbf{r}')d^3\mathbf{r}'+\left[\frac{dn(\mathbf{r},t)}{dt}\right]_i-A_\lambda n(\mathbf{r},t) . \tag{22}$$

Since only the first term on the right-hand side in Eq. (22) is new to the radiation diffusion problem, we consider only that term [to be labeled term 1 ($\mathcal{T}_1$)]. To put term 1 in the same form as the second term (the Holstein term), one needs only to substitute the full expression for the flux F given in Eqs. (17)–(21). For the slab geometry we present results with the x' and y' coordinates explicitly integrated, as discussed above.

Term 1 of Eq. (22) can be reduced by first separating the two surface integrals at $\pm L/2$. The surface integrals are performed as in Eq. (18) above. These integrations introduce several exponential integrals into the equation. Also note that the reflectivity and flux are spatial constants on either surface (see Fig. 1). The following result is obtained after substituting from Eqs. (17), (18), and (20):

$$\mathcal{T}_1=A_\lambda\int dz'n(z')K_{\mathbf{R}}(z,z') , \tag{23a}$$

$$K_{\mathbf{R}}(z,z')=\int d\nu\frac{k(\nu)^4}{\kappa(1-R_+R_-I_L^2)}(T_++T_-) , \tag{23b}$$

where T_+ and T_- are given by

$$T_+=R_+\sqrt{a_+}E_2(k(\nu)\sqrt{a_+})$$
$$\times\{\sqrt{a'_+}E_2(k(\nu)\sqrt{a'_+})$$
$$+R_-I_L\sqrt{a'_0}E_2(k(\nu)\sqrt{a'_-})\} \tag{23c}$$

$$T_-=R_-\sqrt{a_-}E_2(k(\nu)\sqrt{a_-})$$
$$\times\{\sqrt{a'_-}E_2(k(\nu)\sqrt{a'_-})$$
$$+R_+I_uL\sqrt{a'_+}E_2(k(\nu)\sqrt{a'_+})\} . \tag{23d}$$

Equation (23b) represents the part of the kernel to the radiation diffusion problem which is due to the reflective boundaries $K_{\mathbf{R}}(z,z')$, as mentioned after Eq. (1). The corresponding $K_0(z,z')$ term is given below for completeness:

$$K_0(z,z')=\int d\nu\frac{k^2(\nu)}{2\kappa}E_1(k(\nu)\sqrt{a_0}) , \tag{24}$$

$$a_0=(z-z')^2 . \tag{24a}$$

Equations (23) and (24) combined give $K(z,z')=K_0+K_R$. Thus we have a complete description of the radiation diffusion equation for an infinite slab geometry with diffusely reflecting sides with different reflectivities, for conditions of complete frequency redistribution.

In principle, more complicated boundary reflectivity functions can be dealt with. However, the derivation of the appropriate flux functions for a general set of conditions presents a challenging numerical problem. One method of numerical solution to the case we have considered will be discussed below.

C. Line competition effects

We now briefly consider the additional complication of line competition, where two or more trapped transitions deplete the excited state. The calculations to be presented below apply to conditions where the atomic vapor has trapped transitions and is enclosed in a cell appropriate to the discussion given above (see Fig. 1). We discuss the thallium vapor system for the present set of calculations. This system is being examined as a narrow-bandwidth fluorescence filter. The relevant energy levels are shown in Fig. 2. In our thallium atomic resonance fluorescence filter the metastable $6\,^2P_{3/2}$ state is populated by a cw laser at 1.283 μm. In order for the filter to have high conversion efficiency, we must require that the $6\,^2P_{3/2}$ density be maintained at a significant fraction of the total atom density. Our calculations are not restricted to this condition and cover a broad range of densities for both the ground and metastable states. For conditions which are practical to filter operation, where the $6\,^2P_{1/2}$-$7\,^2S_{1/2}$ transition at 378 nm is optically thick, the transition at 535 nm is also optically thick, and thus trapped. For the purpose of the present discussion it is assumed that such conditions are achievable in the vapor. Additionally, the metastable-state density is assumed to be uniform throughout the cell. This is a realistic assumption in our case sine the 1.283-μm transition is very weak. The laser at 1.283 μm is uniform in intensity as it passes through the vapor. We note that a nonuniform metastable-state (or ground-state) density can be dealt with in principle. The optical depth for a photon going from $\mathbf{r}$ to $\mathbf{r}'$ must be calculated explicitly. This will require much more computer time. For a uniform density profile the optical depth is proportional to the path length regardless of where in the cell a photon is emitted or absorbed.

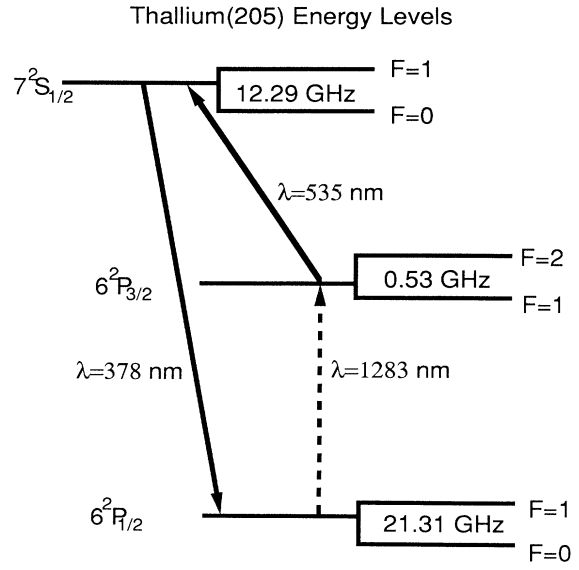

FIG. 2. The thallium-205-isotope energy levels including hyperfine structure due to coupling to the nuclear spin. The transitions at 535 and 378 nm are electric dipole allowed. The transition at 1.283 mm is electric dipole forbidden but is magnetic dipole allowed.

The incorporation of two isolated trapped transitions can be handled with only minor modifications to the radiation diffusion equation. The following expression is valid for the present case:

$$\frac{\partial n(z,t)}{\partial t} = -A_{378}n(z,t) - A_{535}n(z,t) + A_{378}\int dz' K_{378}(z,z')n(z',t) + A_{535}\int dz' K_{535}(z,z')n(z',t) + \left[\frac{dn(z,t)}{dt}\right]_i . \tag{25}$$

For each term, $K(z,z')$ differs only in the range of the frequency integral in Eqs. (23) and (24), and the frequency dependence in the reflectivity. The above equation has been written for the one-dimensional case we consider here, but is also a valid extension for three dimensions: simply replace z with $\mathbf{r}$ and K with G. It is clear that Eq. (25) can be generalized to account for any number of transitions from the excited state.

An error can occur if one assumes that the trapped lifetime of the excitation for either transition can be handled independently. For example, given a cell which approximates an infinite slab geometry with nonreflective surfaces, one might be tempted to use the simple closed-form Holstein expressions [2,3]. Even in this case (with nonreflecting walls), the Holstein solutions may not be valid. Each of the two transitions leads to a different description for the excited-state profile (due to different line shapes, densities of the lower states, and dominant line-broadening mechanisms). There is, however, only a single excited state. The overall or coupled excited-state profile must incorporate the effect of emission and absorption on all of the transitions. Failure to properly consider the effect of all transitions on the excited-state profile can lead to large errors in predicting the decay rate of the excitation, or the ratio of emission of any two transitions. Proper consideration of this effect is even more important when using a cell with reflective boundaries which are different for each of the transitions (such as for the case we consider; see Fig. 1). For this case the excited-state profiles can change dramatically given only a small change in the absorbing state densities.

D. Numerical solution

The radiation diffusion equation as shown in Eq. (25) along with the kernel derived here in Eqs. (23) and (24) can be solved by first using the following mode expansion:

$$n(z,t) = \sum_\alpha C_\alpha n_\alpha(z)\exp(-\beta_\alpha t) . \tag{26}$$

Substituting this into Eq. (25) and rewriting the integral as a summation leads to the following eigenvalue equation:

$$\lambda_\alpha n_\alpha(z_i) = \sum_j K(z_i,z_j')n_\alpha(z_j')\Delta z_j' , \tag{27}$$

with

$$K(z_i,z_j')=\frac{A_{378}K_{378}(z_i,z_j')+A_{535}K_{535}(z_i,z_j')}{A_{378}+A_{535}} . \quad (27a)$$

The kernel has been replaced by the appropriate multiple transition kernel which corresponds to Eq. (25). The spatial modes $n_\alpha(z_j')$, correspond to the eigenvector for the mode α, and λ_α to the eigenvalue of Eq. (27). The escape factor is typically more convenient to describe the decay of excitation than the eigenvalue. Throughout the remainder of the paper we will refer primarily to the escape factor when discussing the decay of a given mode. The escape factor is simply related to the eigenvalues or decay rates:

$$g_\alpha=1-\lambda_\alpha=\frac{\beta_\alpha}{A_{378}+A_{535}} . \quad (28)$$

The integral in Eq. (25) over z' has been expressed as a sum. The escape factor g_α is related to the eigenvalues λ_α and used in the same manner as introduced by Holstein [2,3]. The decay rate for the mode α is β_α; g_α is the escape factor which ranges from 1 (for optically thin conditions where there is no trapping) to ~ 0 (for conditions of high optical depth). For the fundamental mode, $(g_1)^{-1}$ roughly represents the average number of absorptions occurring before a photon escapes from the cell. The eigenvectors represent the distribution of excited-state atoms across the cell for the given mode.

III. RESULTS AND DISCUSSION

The calculations to be presented here represent the initial steps toward developing a model for a narrow-bandwidth thallium fluorescence atomic resonance filter. In order to understand the properties of this filter as a function of buffer gas pressure and ground-state and metastable-state densities; the radiation trapping problem must be well understood. In this section we present some of the calculated decay rates and the excited- ($7S$) state atom profiles for this system. Further details, such as the efficiency of the filter, will be presented in another paper devoted to narrow band atomic resonance filters in thallium. We note here that in general the efficiency is not simply related to the decay rates. To determine the efficiency, one must include the contribution of enough modes [as given in Eq. (26)] to build up the excited-state pump profile (or source term as described above). Then the contribution of each mode must be integrated to give the resulting flux of 378-nm light incident on the surface where the light is collected.

The calculations are done for thallium vapor contained in a cell which approximates an infinite slab geometry (the surfaces parallel to z are considered to be 100% reflecting at all relevant frequencies). The sidewalls (perpendicular to z) where escape occurs are described by four different reflectivities: for each surface and each transition (Fig. 1). For the present calculations the $-L/2$ wall of the slab has

$$R(-L/2,535\text{nm})=0$$

and

$$R(-L/2,378\text{ nm})=100\% ,$$

and on the $+L/2$ wall we have converse conditions with

$$R(+L/2,378\text{ nm})=0$$

and

$$R(+L/2,535\text{ nm})=100\% .$$

We consider a range of optical depths relevant to the filter operation. In addition, we consider much higher and lower optical depths than are practical for high-efficiency filter operation in order to examine the effects of radiation trapping in this system.

A Voigt function is used to model the line shape at a temperature of 700 K. The hyperfine structure due to the coupling with nuclear spin is taken into account [24,25]. One must take care to give the appropriate weighting to the transitions between the hyperfine components. Theoretical selection rules and intensity rules were used from Ref. [26]. The calculations are done for only the more abundant 205 isotope. The inclusion of both isotopes would require a more complicated treatment due to the effects of incomplete frequency redistribution [10,11,14–16]. Note that Doppler broadening tends to obscure the separation in components which arise from the splitting in the metastable level. This splitting is on the order of 1 GHz, as is the Doppler width.

We have considered the effect of buffer gas (argon) in the calculations to ensure that complete frequency redistribution is always a valid assumption (for a single component line shape). References [11] and [12] discuss in detail the conditions for which complete frequency redistribution is a valid assumption. Additionally, some amount of buffer gas is necessary to reduce wall quenching of the metastable $6P_{3/2}$ state. The buffer gas increases the time it takes for thallium atoms to reach the wall. This leads to a long metastable-state lifetime and thus reduces the power needed at 1.283 μm to maintain the required metastable densities for high-transmission filter operation. The foreign gas broadening rates are taken from Refs. [27] and [28] and scaled to the appropriate temperature (700 K is used here). The foreign gas broadening rate coefficients are

$$k_c^{\text{Ar}}(535\text{ nm})=5.83\times10^{-9}\text{ cm}^3\text{s}^{-1} ,$$

$$k_c^{\text{Ar}}(378\text{ nm})=7.01\times10^{-9}\text{ cm}^3\text{s}^{-1} .$$

The self-broadening rate for the 378-nm line is taken from Ref. [29]:

$$k_c^{\text{Tl}}(378\text{ nm})=1.076\times10^{-7}\text{ cm}^3\text{s}^{-1} .$$

Since the broadening occurs in the upper level, the self-broadening rate is assumed to be the same for both the 378- and 535-nm transitions. The full widths of the lines are given by adding the self-broadening contribution to the collisional and natural widths. Note that for the conditions considered here, the self-broadening contribution will usually be small. The absorption profiles are shown in Fig. 3 for both lines given conditions of 5-Torr argon

and a density of 2.0×10^{12} cm^{-3} for each of the two absorbing levels (the optical depth for the full slab thickness is the function plotted, with a full slab thickness of $L=10$ cm).

The eigenvalue problem in Eqs. (27) and (28) has been solved on a Cray X-MP/216 computer. The excited-state density is evaluated at 150 positions throughout the slab. This leads to a 150×150 matrix. First, the 22 500 K-matrix elements are calculated using Eq. (23)–(28). The integrations in x' and y' have already been carried out. The matrix is obviously symmetric (i.e., the probability for a photon emitted at z and being absorbed in the strip around z' is equal to the probability of emission at z' with absorption in the strip around z). The eigenvalues λ_α and eigenvectors n_α are then found using IMSL matrix routines. In principle, a set of these calculations can be done on a reasonably fast personal computer in a couple of days given appropriate matrix-solving routines (this is a rough estimate). However, the 64-bit numbers used by the Cray yield higher accuracy which may be necessary in large matrix calculations.

The eigenvalues (λ_α) are related to the decay rates (β_α) and escape factors (g_α) as shown in Eq. (28). We label the fundamental mode as the first mode; this is the slowest decaying mode. Thus in the late time following a pulsed excitation, the fundamental mode describes the excited-atom profile and decay rate. The higher modes decay successively faster. The matrix routines can produce all 150 modes and corresponding decay rates. However, the higher modes here cannot be expected to be well defined or have accurate decay rates since they oscillate rapidly and are only sampled at 150 points. The first 30 or so modes are defined well enough to be reasonably accurate. The convergence of the escape factor corresponding to these modes was examined as the number of matrix elements was increased and is better than 2% for the highest modes to be used and about 0.1% for the fundamental mode.

We show results for the escape factor of the fundamental mode in Fig. 4 as a function of the 378-nm line-center optical depth (the optical depth is for a single pass through the full slab thickness and is only considered as a plotting parameter). The optical depth on the transition from the metastable level at 535 nm is held constant. The calculations are done for 5 Torr of argon buffer gas, and the metastable-state ($6P_{3/2}$) density fixed at 2×10^{11} cm^{-3}, which corresponds to a Doppler line-center optical depth of 10.115 cm^{-1} (this is k_0L, where $L=10$ cm and k_0 has the usual meaning as given in Ref. [30]). Note that this corresponds to an actual maximum optical depth of 6.117 cm^{-1}, since the maximum absorption is reduced by the hyperfine structure as well as pressure broadening. The length of the slab is 10 cm. Calculations are presented for ground-state densities which range from 3.0×10^{9} to 2.0×10^{13} cm^{-3}. The conditions where the metastable-state density is greater than the ground-state density are not realistic for our proposed pump scheme, but still illustrate some interesting trapping re-

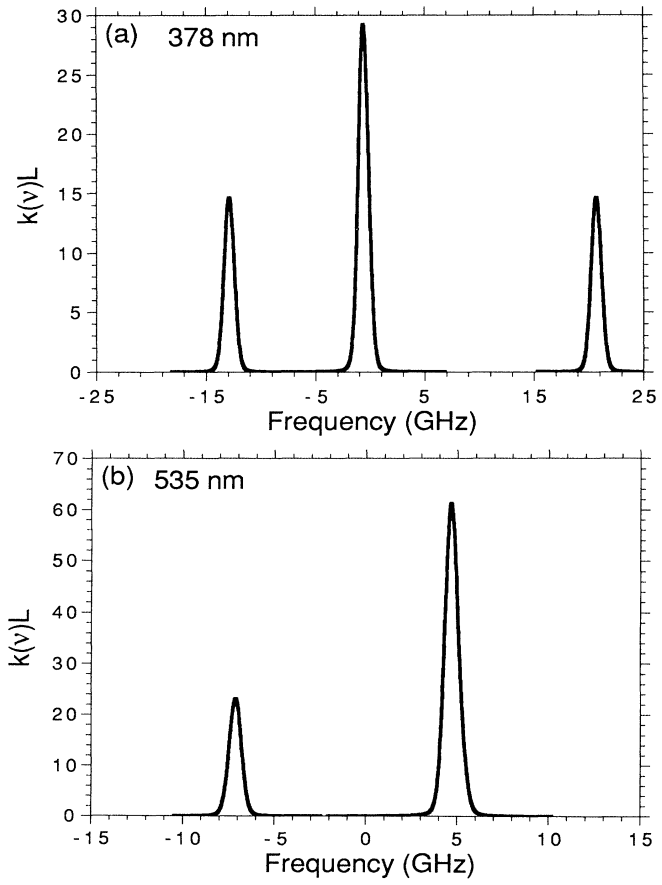

FIG. 3. (a) Thallium 378-nm line shape. The optical depth for a single pass across a cell 10 cm in length is shown as a function of frequency. The ground-state density is 2.0×10^{12} cm^{-3} and argon pressure is 5 Torr. (b) Thallium 535-nm line shape; same density and argon pressure as for the 378-nm line.

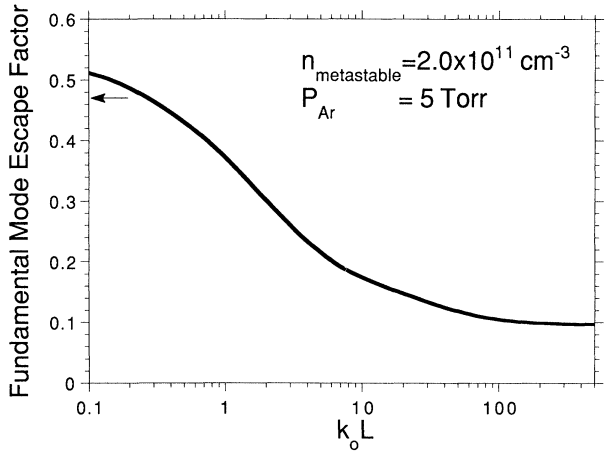

FIG. 4. Fundamental mode escape factor [related to decay rates by Eq. (28)] for a fixed metastable-state density at 2.0×10^{11} cm^{-3} as a function of 378-nm line-center optical depth. The buffer gas is fixed at 5 Torr of argon for both lines. The arrow at the left marks the escape factor corresponding to the 378-nm branching ratio [i.e., $A_{378}/(A_{535}+A_{378})$].

sults. We note that it may be possible top achieve these inversion conditions using other pump schemes [31–33].

The dependence of the fundamental mode escape factor on optical depth is very different than for simpler systems where there is only a single radiating transition. In Fig. 4 we see that the escape factor is bounded at both low and high optical depths. For low optical depth, the optically thin line at 378 nm is emitted without any trapping. Here, the escape factor approaches a value for the corresponding decay rate which is slightly faster than the natural decay rate for the 378-nm transition. The escape factor due only to emission on an untrapped 378-nm line is 0.47, or simply the branching ratio. The fastest escape factor exceeds this in Fig. 4 since there is also some emission on the 535-nm line. Much of the emission occurring at 535 nm is reabsorbed and then has a high probability of being reemitted at 378 nm, where escape occurs. For high optical depths on the 378-nm line, the escape factor is decreased by the trapping on the 378-nm line, but is limited by escape occurring on the 535-nm line which now has the lower optical depth. The escape factor is bounded by the emission from whichever line has a lower optical depth. The behavior of the escape factor at intermediate optical depths is complicated and will depend on the specific system as well as the specific optical depth for each line.

The type of dependence of the fundamental mode escape factor shown in Fig. 4 is expected for a system which has two radiating transitions (the faster decay mechanism dominates the trapping processes and may also dominate the mode structure). The higher modes also may play an important role in the decay process. For example, in order to determine the efficiency of the thallium fluorescence filter at converting 535-nm light to 378 nm, one must sum up the contributions of many modes. The amplitude of each mode is determined by the spatial profile of the source term (or excitation pump profile). The contribution of each mode to the overall escape of photons will depend on the overlap of the spatial distribution of that particular mode with the excitation profile. More on this subject will be discussed in a second paper on the thallium fluorescence filter.

It is important to consider the effect of frequency redistribution in this type of trapping problem. In the Holstein-like equation used here, we make the assumption of complete frequency redistribution [2,3]. That is, a photon absorbed at frequency ν may be emitted at the frequency ν' with probability proportional to $k(\nu')$. In other words, the absorption profile is the same as the emission profile. While there have been several experimental and theoretical studies on the effects of partial frequency redistribution in radiative transfer problems, it remains a complicated aspect to incorporate into the problem [10,11,14–16]. Partial frequency redistribution tends to decrease the escape factor or trapped radiative rate (i.e., it can lead to more trapping than for complete frequency redistribution). Such effects tend to occur over only a limited range of optical depths, which depends on the specific element, line structure, and cell geometry. For purposes of the present discussion, we note that complete frequency redistribution (for redistribution within a single hyperfine component) becomes a valid approximation as soon as only a small amount of buffer gas is included in the cell (about 1 Torr of argon here) [10,11]. (Note that for a single component line, complete frequency redistribution may be valid even with no buffer gas as long as the Doppler-broadening mechanism dominates the trapping for each of the lines considered here. The frequency shift involved in the Doppler effect causes an effective frequency redistribution. However, when a significant fraction of photons escape from the Lorentzian wings of the line, complete frequency redistribution occurs only when the collisional contribution to the Lorentzian linewidth is significantly greater than the natural linewidth.) The inclusion of partial frequency redistribution into the theory developed here would represent a serious complication. We note that this is why we treat only a single isotope of thallium. The two isotopes form a single overall absorption profile; however, one isotope cannot emit a photon with high probability at the line center for the other isotope since the emission profiles of the two isotopes are distinct. In other words, there is no mechanism to convert the 203 isotope to the 205 isotope or the converse (although the excitation can be collisionally transferred by near-resonant collisions, but this transfer rate may be slow). The effect of partial frequency redistribution on systems with two or more trapped transitions will be left for future investigation. We note that the inclusion of buffer gas in our system will be necessary for a fluorescence filter in any case, since this reduces wall quenching of the thallium metastable state.

For the single thallium (205) isotope considered here, the hyperfine structure leads to several components on either of the two lines (see Fig. 3). These components complicate the issue of frequency redistribution. There can be, however, an effective frequency redistribution between these components due to collisional excitation transfer (or collisional mixing). Even for conditions where the absorption profiles of the components appear to be well isolated, the collisional mixing may be complete. Additionally, the effects of line overlap and Doppler shifting can cause an effective mixing between the hyperfine components. For the present set of calculations we assume that there is complete mixing between the various hyperfine levels. The validity of this assumption is discussed below.

There are several mechanisms which can lead to mixing of the hyperfine levels. The mechanisms discussed above can cause mixing of the hyperfine levels either through Doppler shifting, or enhanced line overlap due to collisional broadening. While these mechanisms can be significant under some conditions, they do not guarantee complete mixing. We must also consider the effect of collisional excitation transfer between the hyperfine levels.

We are primarily concerned with excitation transfer collisions involving inert buffer gas. Since the mixing of the ground-state ($P_{1/2}$) hyperfine levels involves a spin flip, the rates may be quite slow. The excited state ($S_{1/2}$) may also be slowly mixed. The metastable-state ($P_{3/2}$) mixing can be much faster since no spin flip is required (i.e., the collision interaction with the orbital angular

momentum is sufficient in this case to cause rapid mixing between the hyperfine F levels).

A lower limit of the cross section of 10^{-17} cm^2 for mixing between the hyperfine levels of the ground state due to collisions with argon has been reported in Ref. [34]. However, Ref. [35] reports a cross section which is about an order of magnitude less than this. The source of this discrepancy is unknown. Using the lower limit from Ref. [34] corresponds to a mixing rate of approximately 10^7 s^{-1} for 500 Torr of argon. This must be compared with the trapped radiative rates of about 10^7 s^{-1}. This corresponds to results shown for higher pressures in Fig. 6; for lower pressure the mixing rate is smaller but the trapped radiative rate also decreases (although not as rapidly). Thus with the lower limit set in Ref. [34] for the cross section, complete mixing in the ground state is a good approximation for sufficient buffer gas pressures. In addition to this mixing mechanism, there may be collisional mixing due to collisions with other ground-state thallium atoms. We estimate that this process represents only a minor contribution to the collisional mixing rate even at the highest thallium densities considered here [36].

The metastable levels ($P_{3/2}$) are mixed at a much faster rate. The rate here is approximately 10^7 s^{-1} for only 1 Torr of argon, using the cross section from Ref. [35]. Additionally, the small splitting in these hyperfine levels allows the Doppler shifting to cause an effective mixing upon reabsorption of photons. The fast mixing in this level can also play a secondary role in further mixing the other levels. Near-resonance collisions between excited-state ($S_{1/2}$) atoms in state i and metastables (or ground-state) ($P_{3/2}$) in state j can result in excited-state atoms in state j and ground-state atoms in state i (i and j refer to a particular hyperfine level). If one considers this cross section to be as large as typical resonance broadening cross sections, then this mechanism can contribute significantly to the mixing for sufficient metastable-state densities (this also depends on the trapped radiative rate). That is, the complete mixing occurring in the metastable state can be transferred to the excited state.

For lack of any experimental measurements on the mixing in the excited state ($S_{1/2}$), we make the assumption that the cross section is at least as large as that for the ground state. Thus for high pressures and only moderate trapping (or low pressures and severe trapping), the excited-state hyperfine levels will be completely mixed (as discussed for the $P_{1/2}$). For conditions where there is low buffer gas pressure and very little trapping, the mixing will of course not be complete. However, in these cases the trapping problem is trivial and the error made by our assumption cannot be very large. For intermediate conditions the effects of partial mixing (thus partial frequency redistribution) are in general too complicated to incorporate directly into the radiation trapping problem.

For conditions where collisional line broadening, collisional mixing, and Doppler shifting effects are not sufficient to give complete frequency redistribution, more complicated radiation diffusion equations must be developed for the present system. While partial frequency redistribution can be quite complicated, the case where there is no mixing between hyperfine components may not be as difficult to deal with as long as the mixing within each isolated component is complete. For thallium, the upper $7S$ level has a relatively large hyperfine level splitting of 12.29 GHz. Thus one might be tempted to treat the hyperfine components as completely isolated. However, even for line-center optical depths (~ 20) across the cell, a significant fraction of the emission from the cell can occur in the overlapping region between these "isolated" components. We note that the frequency profile of emission from the cell is a self-reversed line shape and note the same as the local emission profile. Thus it is predominantly regions of low optical depth, not line-center regions, that contribute to the escape of photons. One must take care to consider this overlap region of the absorption profiles resulting from the hyperfine structure. For somewhat higher densities or buffer gas pressures (a factor of 5 or 10) than used to calculate the line shapes shown in Fig. 3, the optical depth across the cell is between about 0.2 and 1 for much of the overlapping region between the hyperfine components. For such conditions these regions will contribute significantly to the escape of photons from the cell; thus the hyperfine components cannot be considered isolated in this case (and even for the lower pressures and densities considered here, the partial overlap may have a significant effect on the decay rates). If the splitting in the $7S$ level were much larger so that this type of overlap does not occur, the line components might then be considered as isolated; however, then one must deal with separate excited-state populations, decay rates, and mode profiles for each of the isolated energy levels and corresponding transitions. In the converse case, where the ground-state splittings are very large and the levels are unmixed, and the upper state can be considered as a single mixed state, one may consider the resulting transitions to be completely isolated. It is then possible to consider the effect of each isolated transition on the excited-state density and determine an overall excited-atom profile. This is exactly what we have done for the present case with respect to the two $6P$ fine-structure levels, which are considered as an isolated pair of ground-state levels. For the calculations presented here the $7S$ upper-state hyperfine levels are considered completely mixed. We do not consider the cases where the hyperfine components are either partially mixed or not mixed at all.

However, neither the assumption of complete mixing nor that of no mixing between the hyperfine levels is valid for the entire range of conditions considered here. Either of these assumptions simplifies the calculation of the trapped decay rates and mode profiles. We make the assumption that complete mixing does occur for the calculations presented here. This approximation avoids the necessity of calculating separate decay rates and mode profiles for hyperfine levels and the corresponding transitions. In particular for thallium, the densities of each of the hyperfine levels in the excited state would need to be considered. This can also lead to problems with respect to specifying the initial excitation of the system. The complete mixing approximation is certainly valid for either severe trapping conditions or when high buffer gas

pressures are used. Since there are several mechanisms which contribute to the frequency redistribution (both within a single line and between the hyperfine components), the complete frequency redistribution approximation is valid for at least some of the conditions considered here. This approximation also simplifies the description of the system compared to the no-mixing approximation. Our approximation is physically significant since it is likely to be valid (depending on the specific conditions) for conditions where there is significant trapping.

Since the fundamental mode decay rates discussed above do not provide a complete picture of the radiation trapping process in the cell described, we must consider the effect of the higher modes. In order to determine the rate of emission per cm^2 from either line onto either surface, one must consider the total excited-atom profile. This involves determining the contribution from several of the slowest decaying modes. We show the first few of these modes in Fig. 5. The densities are 2.0×10^{12} cm^{-3} for the ground state and 2.0×10^{11} for the metastable state, and 5 Torr of argon is included.

The modes no longer have the symmetry of the cell due to the reflective boundaries. For the densities used to calculate the modes shown in Fig. 5, the 535-nm line is less optically thick. The effect on the fundamental mode is clear: The mode is peaked near the reflective wall for 535-nm light (note that for a system with only one line at 535 nm, the peak of the fundamental mode is actually at the mirrored wall). Only a moderate amount of light can exit the $+L/2$ surface since the 378-nm light (which can only escape at $+L/2$) is heavily trapped. At the $-L/2$ surface, more light can escape from the cell on the 535-nm transition, since this is only moderately trapped. For conditions where both lines are optically thick, the shape

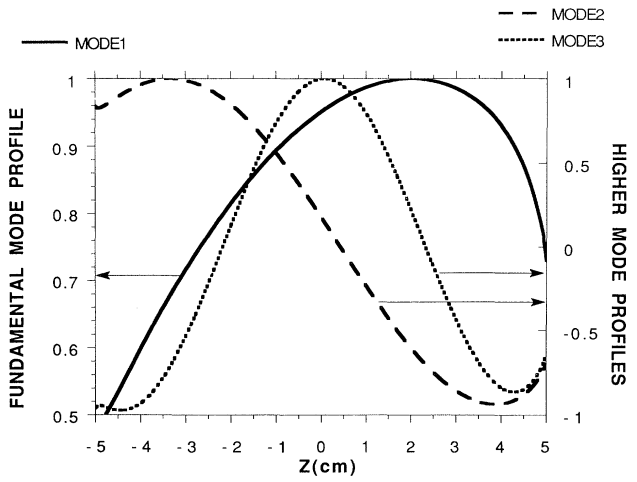

FIG. 5. First three mode profiles for densities of 2.0×10^{11} and 2.0×10^{12} cm^{-3} in the metastable and ground states, respectively. The buffer gas is fixed at 5 Torr of argon. The fundamental (or first) mode is plotted agains the left axis; the two higher modes are plotted against the right axis. The escape factors are 0.111, 0.258, and 0.366 for the first, second, and third modes, respectively.

of the mode depends on the details of the cell and line shapes, and appears to be quite complicated. As long as neither transition is optically thin, the mode structure is dominated by the transition, which leads to faster escape.

The appearance of the modes shown in Fig. 5 can change dramatically by changing either the reflectivities or the densities of the ground or metastable states. For the cell reflectivities we have considered here and with the higher optical depth on the 378-nm line, the peak of the fundamental mode is toward the $+L/2$ surface. For converse conditions on the optical depths of the two lines, the peak will clearly be toward $-L/2$. This contrasts significantly with the typical trapping cases (those considered by Holstein [2,3]) where the appearance of the fundamental mode changes very little regardless of changes in the optical depth [2]. For cases considered by Holstein, the peak of the fundamental mode is always at the center of the cell. The differences in the overall excited-state profile for our case must be considered in order to determine the efficiency of an atomic resonance filter. It is clear that two very different conditions for the optical depth can result in very similar decay rates. The filter efficiency, excited-atom profile, and emission profiles would be very different for such cases.

Since we must use some buffer gas in our system to prevent quenching of the metastable state by the walls, and to ensure complete mixing between the hyperfine levels, we have examined the effect of varying the buffer gas pressure on the fundamental mode decay rates (for argon pressure below 1 Torr, the complete frequency redistribution assumption we make may not be valid for some thallium densities). The fundamental mode escape factors (g_1) are plotted in Fig. 6 as a function of argon pressure for fixed densities of 2.0×10^{12} cm^{-3} in the metastable and ground states. For nonreflective cells, with simple line structure, the escape factor has a square-root dependence on the buffer gas pressure for conditions where collisional line broadening dominates the trapping. For the present case we see similar qualitative behavior. In either case, as pressure is added to the system, the lines broaden and at high enough pressures become optically thin. In this pressure range the escape factor tends toward 1, and there is no trapping. For low pressures, the regions of the line shapes which dominate the radiation trapping (the unity optical depth region of the lines) are in the Doppler core of the line. Thus changing the pressure has only a negligible effect on the escape factor. For conditions of high optical depth, the region between these limits may cover several orders of magnitude in the escape factor. For the present case the lines are just becoming optically thin for the highest pressure shown (the escape factor is already ~0.5). The complicated line structure also has some effect on the pressure dependence due to overlap between the hyperfine components (see Fig. 3). The peak optical depth is reduced due to the hyperfine structure. The hyperfine component line overlap can make the pressure dependence very complicated. This is the cause of the slight unevenness seen in Fig. 6. For the conditions used in Fig. 6 we see that the high and low optical depth limits differ by slightly more than an order of magnitude. Even in this case the dependence of the es-

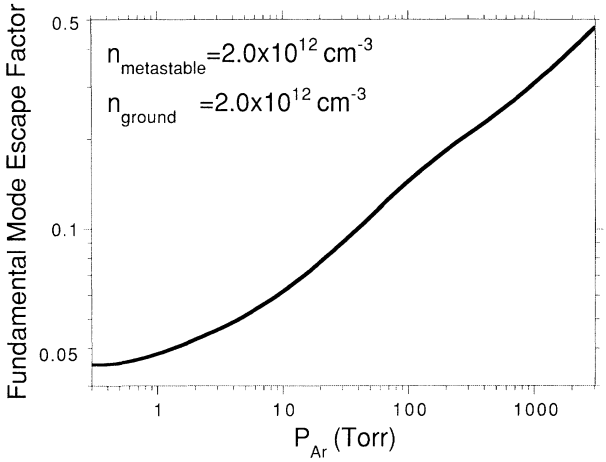

FIG. 6. Fundamental mode escape factor for densities of 2.0×10^{12} cm^{-3} in both the ground and metastable states as a function of argon pressure.

cape factor on pressure in the central region from $P=10$ to 100 Torr approaches the expected square-root pressure dependence (closer to $P^{0.4}$). The small deviations are due to the details of the system. We note that the high-density conditions used for Fig. 6 are probably not appropriate to efficient filter operation. Results for lower densities would not display the pressure dependence over a broad range of escape factor, since even at low pressures there would be very little trapping.

IV. CONCLUSIONS

We have derived a radiation diffusion equation for a cell which approximates an infinite slab with different reflectivities on either surface. We have also included the effects of line competition (multiple trapped transitions). The diffusion equation has been rewritten as an eigenvalue matrix equation which can be solved numerically on a computer. We have examined the thallium vapor system where both the $6\,^2P_{1/2,3/2}$ levels are populated. The effect of the two optically thick transitions at 535 and 378 nm on the upper $7\,^2S_{1/2}$ state has been considered. The cell considered here is described in Fig. 1. This system is being studied as an ultranarrow-bandwidth atomic resonance filter with a wide field of view.

The general derivation given above can incorporate any four reflectivities into the thallium system. It is important to consider the effect of reflectivities which are less than 100% at the surface where light of either transition frequency is allowed to escape. For example, consider the case where the two nonzero reflectivities are now 80% (instead of 100%) and there is a factor-of-10 difference in the optical depth of the two transitions. For this case the additional 20% loss from the optically thinner of the two lines may have a more significant effect than the total emission from the optically thicker line. Similar arguments can be made for a change in reflectivity at the 0% reflecting surfaces. The light reflected back into the cell at one frequency may be more significant than the escape occurring on the second transition. Such minor changes in the reflective boundary conditions would thus be expected to lead to significant changes in both the decay rates and the mode profiles. In order to model accurately the thallium narrow-bandwidth atomic fluorescence filter, these effects may need to be considered in detail. These calculations are outside the scope of this paper.

The fundamental mode decay rate shown in Fig. 4 is clearly limited in both low and high optical depth regions. This behavior is specific to trapping problems which consider two (or more) trapped transitions. The fundamental mode decay rate alone, however, is not sufficient to describe the emission as a function of time and frequency from either side or the cell (this is just the flux exiting the surfaces at either frequency). Several of the slowest decay rates as well as the corresponding mode profiles must be used in order to describe both the excited-state density as a function of time across the cell and the emission as a function of frequency, time, and cell surface. While we have determined these modes (see Fig. 5) and decay rates, we have not discussed how to determine the amplitudes of these modes or how to integrate over the modes to determine the photon fluxes, (i.e., the emission at 535 and 378 nm at either surface). Thus we have completed only the first step in describing fully the thallium fluorescence filter. Further material allowing for determination of the quantum efficiency at converting 535-nm photons to 378-nm photons will be discussed in a separate paper devoted to thallium filters.

There has been very little work done on radiation diffusion which discusses the effects of multiple trapped transitions. Two other groups are also examining different filter concepts in thallium vapor systems and thus must deal with the radiation trapping problem [31–33,37]. Each of the suggested thallium filters uses a different technique to populate the metastable state. The radiation diffusion problem for the thallium fluorescence filter system described here in Fig. 1 has also been examined in detail in Ref. [32]. The nature of their solution to the problem of the three-level thallium system in the cell of Fig. 1 differs significantly from our own. In their work [31,32] the coupled modes (for the three-level system we consider) are described as an expansion of the normal two-level Holstein modes [2,3] (i.e., the kernel to the radiation diffusion equation is the same as that used by Holstein). The modes for an infinite slab found using the normal two-level Holstein kernel can be simply related to those for a cell of half the width, with one side being 100% reflective. There is no way to incorporate partially reflective surfaces without deriving an appropriate kernel to the radiation diffusion equation, as we have done here. The solution of Ref. [32] may, for some conditions, be computationally less complicated than our own. We believe our work represents the most general treatment of the radiation diffusion problem for this type of system. The theory presented allows one to incorporate several transitions to lower states as well as the effect of partially reflective surfaces. We have also discussed how to handle the effects of frequency redistribution within a single

component of a transition, and the effects of collisional mixing between hyperfine components. The spatial modes presented here in Fig. 5 are unique in that these modes no longer reflect the symmetry of the cell in a simple manner. This is a result of the inclusion of different reflective boundaries on either of the two slab surfaces and dealing with emission at more than a single frequency range.

ACKNOWLEDGMENTS

One of the authors (T.M.C.) is grateful to Dr. A. Streater for very helpful discussions on radiation diffusion problems early on this work and for initially suggesting how to apply the matrix style of solution to this type of problem. This research was supported by the Office of Naval Technology.

*Present address: Department of Chemistry and Physics, Augusta College, Augusta, GA 30910.

[1] E. Milne, J. London Math. Soc. **1**, 1 (1926).
[2] T. Holstein, Phys. Rev. **72**, 1212 (1947).
[3] T. Holstein, Phys. Rev. **83**, 1159 (1951).
[4] A. V. Phelps, Phys. Rev. **110**, 1362 (1958).
[5] M. A. Weinstein, J. Appl. Phys. **33**, 587 (1962).
[6] B. P. Kibble, G. Copley, and L. Krause, Phys. Rev. **153**, 9 (1967).
[7] J. H. Ingold, J. Appl. Phys. **39**, 5834 (1968).
[8] J. H. Ingold, J. Appl. Phys. **94**, 94 (1970).
[9] D. Mihalas, *Stellar Atmospheres* (Freeman, San Francisco, 1970).
[10] M. G. Payne and J. D. Cook, Phys. Rev. A **2**, 1238 (1970).
[11] M. G. Payne, J. E. Talmage, G. S. Hurst, and E. B. Wagner, Phys. Rev. A **9**, 1050 (1974).
[12] C. van Trigt, Phys. Rev. A **13**, 726 (1976).
[13] R. P. Blickensderfer, W. H. Breckenridge, and J. Simons, J. Phys. Chem. **80**, 653 (1976).
[14] H. A. Post, Phys. Rev. A **33**, 2003 (1986).
[15] H. A. Post, P. van der Weijer, G. S. Hurst, and E. B. Wagner, Phys. Rev. A **33**, 2017 (1986).
[16] A. Streater, J. Cooper, and W. Sandle, J. Quant. Spectrosc. Radiat. Transfer **37**, 151 (1987).
[17] J. Huennekens, H. J. Park, T. Colbert, and S. C. McClain, Phys. Rev. A **35**, 2892 (1987).
[18] A. Romberg and H. J. Kunze, JQRST **39**, 99 (1988).
[19] M. L. Yanson, V. B. Grushevskii, and Ya. P. Klyavinsh, Opt. Spektrosk. **67**, 522 (1989) [Opt. Spectrosc. (USSR) **67**, 305 (1989)].
[20] J. Huennekens and T. Colbert, J. Quant. Spectrosc. Radiat. Transfer **41**, 439 (1989).
[21] T. Colbert and J. Huennekens, Phys. Rev. A **41**, 6145 (1990).
[22] W. Falecki, W. Hartmann, and R. Bocksch, Opt. Commun. **83**, 215 (1991).
[23] T. Colbert and J. Huennekens, Phys. Rev. A **44**, 4753 (1991).
[24] A. Flushberg, T. Mossberg, and S. R. Hartmann, Phys. Rev. A **14**, 2146 (1976).
[25] A. L. Odintsov, Opt. Spectrosc. (USSR) **9**, 75 (1960).
[26] H. G. Kuhn, *Atomic Spectra* (Longmans, Green & Co., London, 1969).
[27] B. Cheron, R. Scheps, and A. Gallagher, Phys. Rev. A **15**, 651 (1977).
[28] B. Cheron, R. Scheps, and A. Gallagher, J. Chem. Phys. **65**, 326 (1976).
[29] J. C. Hsieh and J. C. Baird, Phys. Rev. A **6**, 141 (1972).
[30] A. C. G. Mitchell and M. W. Zemansky, *Resonance Radiation and Excited Atoms* (Cambridge University, Cambridge, England, 1934).
[31] G. Magerl (private communication).
[32] A. F. Molisch, B. P. Oehry, W. Schupita, and G. Magerl Opt. Commun. (to be published).
[33] B. P. Oehry, W. Schupita, and G. Magerl, Opt. Lett. **16**, 1620 (1991).
[34] F. A. Franz, G. Leutert, and R. T. Shuey, Helv. Phys. Acta **40**, 778 (1967).
[35] H. M. Gibbs and G. C. Churchill, Phys. Rev. Lett. **25**, 263 (1970).
[36] N. Beverini, P. Minguzzi, and F. Strumia, Phys. Rev. A **4**, 550 (1971).
[37] C. S. Liu, P. J. Chantry, and C. L. Chen, Proc. Soc. Photo-Opt. Instrum. Eng. **709**, 132 (1986).